# Polyelectrolyte chain dimensions and concentration fluctuations near phase boundaries

V. M. Prabhu and M. Muthukumar[a)]
*Department of Polymer Science and Engineering, Materials Research Science and Engineering Center, University of Massachusetts, Amherst, Massachusetts 01003*

G. D. Wignall and Y. B. Melnichenko
*Oak Ridge National Laboratory, Condensed Matter Sciences, Oak Ridge, Tennessee 37831-6393*

(Received 20 March 2003; accepted 23 May 2003)

We have measured the temperature ($T$) dependence of the correlation length ($\xi$) for concentration fluctuations in aqueous solutions of sodium–poly(styrene sulfonate) with a fixed level of added barium chloride salt. Apparent critical behavior is observed upon lowering the temperature to precipitation phase boundaries that complements our earlier work on salt-dependent behavior. We interpret experimental deviations from $\xi^{-2}$ versus $T^{-1}$ as crossover from the mean field to the Ising universality class. We also measured the radius of gyration ($R_g$) of labeled chains and $\xi$ for semidilute polyelectrolyte solutions at low ionic strengths. We recovered the familiar result of $\xi$ scaling with polymer concentration ($C_p$) and degree of polymerization ($N$), such that $\xi=(73\pm 9)N^0C_p^{-0.48\pm 0.03}$ [Å], and using SANS high concentration labeling $R_g=(400\pm 28)C_p^{-0.24\pm 0.01}$ [Å] (for $N=577$) and $R_g=(2.8\pm 2.1)N^{0.6\pm 0.1}$ [Å] (for $C_p=206$ gL$^{-1}$), respectively. The indices recovered are in agreement with theoretical predictions for low ionic strength semidilute solutions. Such experiments offer insight into relatively unexplored phase behavior in charged macromolecular solutions. © *2003 American Institute of Physics.* [DOI: 10.1063/1.1592496]

## I. INTRODUCTION

Equilibrium properties of polyelectrolytes remain a significant challenge both experimentally and theoretically. Experimental techniques such as static and dynamic light scattering measure the collective behavior of the static structure and relaxation modes.[1] Specific to polyelectrolytes, these experiments reveal a long-time scale relaxation mode coupled to a short-time scale relaxation,[2–4] the slow and fast modes, respectively. The origin of the slow mode has been attributed to a static multichain aggregate, while the fast mode is attributed to the coupled diffusion of polyion and counterions. The aggregation behavior has been explored and new results have revealed that the size scale is significantly greater than the single chain dimensions using a combination of experimental techniques such as light and neutron scattering.[5,6] However, the molecular origins that lead to such aggregation processes in low ionic strength solutions and connection to thermodynamic polyelectrolyte phase diagrams remain lacking. Many experiments have demonstrated phase diagrams for polyelectrolytes in the presence of added salts.[7–14] These precipitation diagrams, typically plotted as added salt concentration versus polymer concentration show similar features for a variety of polyelectrolytes including flexible and semiflexible polyelectrolytes. Strong theoretical efforts have been put forth to understand the effect of multivalent ions on the phase diagrams of flexible polyelectrolytes.[7,15] However, the theories do not consider the specific influence of added salts on the configurational properties. Yet, some progress is made regarding the general shapes and trends of phase diagrams in understanding experiments.[7]

The role of temperature on aggregation and precipitation behavior has not received sufficient attention. This is surprising considering inverse temperature times molecular weight determines the state of miscibility for neutral polymers in the form of $\chi N$, where $\chi$ is the Flory–Huggins interaction parameter and $N$ the degree of polymerization. Such behavior should also be observed with polyelectrolytes. However, it may be masked by the proximity of the phase diagram and relatively small experimental window of temperature that aqueous solutions are able to be examined, as opposed to polymer melts.

In this paper, we study aqueous solutions of sodium–poly(styrene sulfonate) (NaPSS) with the added salt barium chloride. We explore the homogeneous phase by investigating the effects of added salt concentration versus polymer concentration ($C_s-C_p$) and temperature versus polymer concentration ($T-C_p$). To address the collective properties we have utilized small-angle neutron scattering (SANS) to measure the correlation length ($\xi$) and osmotic compressibility, proportional to the scattered intensity extrapolated to zero angle, $\propto I(0)$, as functions of degree of polymerization ($N$), polymer concentration ($C_p$), added salt concentration ($C_s$), and temperature. The experiments focus in the limit of both low ionic strength and high ionic strength. Comparison of the experimental data for $\xi$ is made with respect to the anticipated scaling behavior of $\xi(C_p,N)$ in the low ionic strength regime and $\xi(C_s,C_p,T)$ and $I(0)(C_s,C_p,T)$ in the high ionic strength regime. To address the configurational properties, we use the high concentration labeling technique

a)Author to whom correspondence should be addressed. Electronic mail: muthu@polysci.umass.edu

 

to measure the size of labeled chains in semidilute solution as functions of molecular weight, polymer concentration, and added salt concentration. The expectation of strong coil contraction with added multivalent salts is compared within the limits of extended-chain conformations and Gaussian coils; globular dimensions are not experimentally achieved. The scaling behavior of $R_g$ $(C_p, N)$ is determined for the case of no added salt, and the results are consistent with scaling laws[16] and the double screening theory[17] for semidilute solutions.

The rest of the paper is organized as follows: Section II describes our experimental protocols covering the SANS methodology in Sec. II A, sample preparation in Sec. II B, methodology for determining the $C_s-C_p$ and $T-C_p$ phase diagrams in Sec. II C. Experimental results are given in Sec. III. Collective properties and labeled chain behavior are discussed in Secs. IV and V, respectively. Section VI contains major conclusions.

## II. EXPERIMENT

Here we will briefly describe the origin of the samples, the protocol to prepare samples for the neutron scattering, method of determining the temperature-dependent phase diagrams, and the SANS high concentration labeling methodology.

### A. Small-angle neutron scattering

We refer to the main results of the high concentration methodology for the two component solutions used previously,[14,18,19]

$$I(q)=I_s(q)+I_t(q), \tag{1}$$

$$I_s(q)=KnN^2S_s(q), \tag{2}$$

$$I_t(q)=LnN^2S_t(q), \tag{3}$$

with prefactors,

$$K=[b_h-b_d]^2x_h(1-x_h),$$

$$L=[b_hx_h+b_d(1-x_h)-b_s']^2.$$

The absolute differential coherent scattering cross section, $I(q)$, in units of $\mathrm{cm}^{-1}$, in this method is composed of a sum of two types of scattering; scattering associated with intrachain monomer–monomer correlations $(I_s)$ and total scattering from all monomer–monomer correlations $(I_t)$, both intrachain and interchain. $b_h$ and $b_d$ are the scattering lengths of the protonated and deuterated monomers, respectively. $b_s'$ is the scattering length of a solvent molecule normalized via the ratio of the specific volume of the monomer and solvent molecule. The average scattering length of the solvent, $b_s'$, may be adjusted by using a mixture of $H_2O$ and $D_2O$ such that $b_s'=y_hb_{H_2O}+(1-y_h)b_{D_2O}$, where $y_h$ is the mole fraction of $H_2O$ and $b_{H_2O}$ and $b_{D_2O}$ are the pure component scattering lengths. $n$ is the number of polymer molecules per unit volume of solution. The essential physics concerning the configurational properties remains in the single-chain structure factor $(S_s)$, and the collective properties in the total scattering structure factor $(S_t)$. The single chain scattering may be directly measured by making the prefactor $L$ to the intensity of total scattering go to zero. We will refer to the matching point as the condition such that the average scattering length density[20] of the monomer matches that of the solvent which gives $L=0$.

The SANS experimental results reported here were performed at three different neutron scattering facilities; the W. C. Koehler SANS facility at the Oak Ridge National Laboratory (ORNL),[21] the National Institute of Standards and Technology (NIST) Center for Neutron Research facility (NCNR),[22] and at the FRJ-2 research reactor of the Forschungzentrum Jülich, Germany.[23]

At the W. C. Koehler SANS facility at ORNL, measurements were made using a neutron wavelength of 4.75 Å with wavelength distribution of $\Delta\lambda/\lambda\approx5\%$. The scattered neutrons were collected with a two-dimensional area detector using a sample-detector distance of 5.8 m. The neutron count rate was corrected for instrumental backgrounds and detector efficiency on a cell-by-cell basis prior to radial averaging resulting in a $q$ range of $0.008<q<0.1$ Å$^{-1}$, where $q$ is the scattering wave vector defined by $q=4\pi\lambda^{-1}\sin(\theta/2)$, where $\theta$ is the scattering angle. The net intensities were converted to an absolute ($\pm4\%$) differential cross section per unit sample volume (in units of $\mathrm{cm}^{-1}$) by comparison with precalibrated secondary standards, based on the measurement of beam flux, vanadium incoherent cross section, the scattering from water and other reference materials.[24] Procedures for calculating the incoherent background, arising largely from the protons in the sample, have been described previously.[25]

At the NG3 30 m SANS facility at the NCNR, measurements were made using a neutron wavelength of 6.0 Å with wavelength distribution of $\Delta\lambda/\lambda\approx15\%$. Two configurations, a 10 m and 3.8 m sample-detector distance, were used leading to an overlapping $q$-range of 0.005 to 0.0595 Å$^{-1}$ and 0.0218 to 0.337 Å$^{-1}$, respectively. The measured neutron count rate, across a two-dimensional area detector, was normalized per $10^8$ monitor counts and corrected for detector efficiency, cadmium blocked beam background, and empty cell scattering on a cell-by-cell basis in accord with NIST's standard procedure. These net intensities were then converted to an absolute differential cross section per unit sample volume (in units of $\mathrm{cm}^{-1}$) using a light water reference material.

At the KWS-II 40 m SANS beam line, FRJ-2 research reactor of the Forschungzentrum Jülich, Germany, measurements were conducted using a neutron wavelength of 7 Å. Three separate configurations were used: 20 m, 8 m, and 2 m. The scattered intensity data were reduced in a manner similar to that at ORNL as the scattered neutrons were collected across a two-dimensional area detector and the neutron count rate was corrected for detector sensitivity, cadmium blocked beam background, and empty cell scattering prior to radial averaging. The net intensities were converted to an absolute ($\pm4\%$) differential cross section per unit sample volume (in units of $\mathrm{cm}^{-1}$) by comparison with precalibrated secondary standards, based on the measurement of beam flux, vanadium incoherent cross section, the scattering from water and other reference materials.[24]

TABLE I. Polymer characteristics.[a]

| | Parent PS | | | Sulfonated NaPSS | | |
|---|---|---|---|---|---|---|
| Name | $M_n$ [g mol$^{-1}$] | PDI | $N_n$ [monomers/chain] | $N^{SANS}$ [monomers/chain] | %S(E.A.) | SANS Facility |
| *h*-NaPSS-82 | 8565$^{(2)}$ | 1.03 | 82 | | 97 | ORNL |
| *h*-NaPSS-234 | 24 350$^{(3)}$ | 1.02 | 234 | | 100 | ORNL |
| *d*-NaPSS-274 | 28 500$^{(2)}$ | 1.03 | 274 | 280±14 | 92 | ORNL |
| *h*-NaPSS-287 | 29 800$^{(1)}$ | 1.02 | 287 | 280±14 | 96 | ORNL |
| *d*-NaPSS-563 | 63 000$^{(2)}$ | 1.05 | 563 | 626±30 | 86 | NIST |
| *h*-NaPSS-577 | 60 000$^{(3)}$ | 1.02 | 577 | 626±30 | 89 | NIST |
| *d*-NaPSS-958 | 107 300$^{(2)}$ | 1.04 | 958 | 979±60 | 86 | FRJ-2 |
| *h*-NaPSS-962 | 100 085$^{(3)}$ | 1.05 | 962 | 979±60 | 88 | FRJ-2 |
| *h*-NaPSS-1990 | 207 000$^{(2)}$ | 1.05 | 1990 | | | FRJ-2 |

[a]$N_{SANS}$ are averaged over all polymer concentrations and salt concentrations for each molecular weight. $M_1^{d\text{-PS}}=112$ g mol$^{-1}$ and $M_1^{h\text{-PS}}=104$ g mol$^{-1}$. Parent PS samples were obtained from (1) Polymer Labs, (2) Polymer Source, or (3) MRSEC-University of Massachusetts.

### B. Sample preparation

We have prepared several molecular weights of deuterated and protonated sodium–poly(styrene sulfonate) by sulfonating poly(styrene)s from Polymer Source, Polymer Laboratories, and MRSEC facilities at the University of Massachusetts–Amherst. We have outlined the typical sample preparation in our earlier publication for sulfonation of low polydispersity parent poly(styrene)s.[14] However, we make one modification here; following the sulfonation and separation of the aqueous polymer rich phase the solution is passed through a column of 400 cm$^3$ of Dowex MR-3 mixed bed ion-exchange resin, purchased from Sigma–Aldrich, followed by an equivalent amount of Milli-Q UF quality water. The ion-exchange method was preferred over dialysis due to the large volumes of fluids encountered and rapid purification. The ion-exchange resin was rinsed thoroughly with deionized water and agitated to remove any low molar mass impurities, after which the effluent water is checked for low conductance and light scattering to ensure removal of contaminants. After ion exchange of the polymer solution, the clear acidic solution is then filtered through a 0.45 $\mu$m cellulose acetate filter unit manufactured by Corning Costar. Subsequent neutralization of the acidic protons was achieved by titrating with a sodium hydroxide solution purchased from Fisher Scientific, certified 0.201–0.199N. At this point we checked the concentration of polyelectrolyte by UV spectroscopy and compared this to the concentration estimated by titration, achieving quantitative agreement. This solution was then filtered through a 0.22 $\mu$m cellulose acetate filter unit manufactured by Corning Costar followed by freezing and lyophillization. After lyophillization, the samples were further dried under a purge of dry $N_2$ in an oven at 105 °C for 1th. Following this procedure, thermogravimetric analysis (TGA) was performed and repeatedly reveal a reversible mass loss, attributed to water.

Table I contains the information regarding the protonated and deuterated molecular weight matching required for the high concentration labeling experiments as well as the characterization details regarding the parent poly(styrene)s and sulfonation levels determined by elemental analysis (EA). We provide the degree of polymerization obtained from SANS as well as the neutron scattering facility indicated as ORNL, NIST, or FRJ-2. We will refer to the degree of polymerization ($N$) rather than molecular weight in order to be consistent from sample to sample as the degree of sulfonation varies leading to an uncertainty in molecular weight. Samples related to correlation length measurements will be refered to as the corresponding *h*-NaPSS-*N*, whereas labeled chain experiments, *d*-NaPSS-*N*, where $N$ is the degree of polymerization.

The general scheme for SANS sample preparation is to use protonated Na–poly(styrene sulfonate) (*h*-NaPSS) in deuterium oxide solutions for the total scattering experiments. For the high concentration labeling experiments we use a fixed mass fraction of *h*-NaPSS of 0.40 ($x_h=0.40$), and the balance deuterated NaPSS. Then we mix these with the solvent mixture of $D_2O$ and $H_2O$ such that the volume fraction of $H_2O$ is 0.32 ($y_h=0.32$). For barium chloride salt containing experiments, we always use stock salty solutions, which can be prepared with accuracy. The $H_2O$ used in this study is of Milli-Q UF Plus System quality with resistivity of 18 MΩ cm. The $D_2O$ is from Cambridge Isotope Laboratories, Inc., (99.9%). The barium chloride salt, purchased from Fisher-Scientific, used in this study is a di-hydrate ($BaCl_2 \cdot 2H_2O$) under ambient conditions, but was dried to remove water by heating to 140 °C for 24 h.

To prepare samples, a predetermined mass of polyelectrolyte, accounting for adsorbed water, is added to plastic centrifuge vials to facilitate easy transfer, as the solutions do not wet these containers, thus minimizing loss of material. For the case of samples which do not exhibit precipitation at room temperature, we add an appropriate volume of salt-free or salty stock solution to the vials and then agitate with a vortexer. These samples may then be transferred using an Eppendorf Pipet-man into the required quartz cuvettes for SANS. However, for samples which exhibit precipitation we use an alternative method. A fixed volume of salt-free solution is added to the dried polyelectrolyte. Then an amount of this polymer solution equal to half the volume of the cuvette is added to the cuvette. We then add a concentrated salty

solution of equivalent volume directly to the quartz cuvette, such that precipitation occurs only within the controlled volume. This is then subsequently heated and mixed with the aid of a vortexer. The reason for this protocol is that it is not possible to transfer a precipitated solution with reliability of the final concentrations. As an example, to prepare a solution with final barium chloride concentration of 0.25 M and NaPSS concentration of 103 $gL^{-1}$, 0.325 mL of $D_2O$ was added to 73.65 mg, this was then mixed and 0.300 mL was transferred to a quartz cuvette with path length 2 mm and diameter 2 cm. Then 0.300 mL of 0.50 M barium chloride salt containing solution is added directly into the SANS cuvette. Identical sample preparation was used for the labeled chain studies, except that we use $x_h=0.40$ and $y_h=0.32$. To investigate polymer concentrations greater than 206 $gL^{-1}$, we account for the absorbed $H_2O$ as adjusting the $D_2O/H_2O$ mixture. Thus we prepare specially a stock solvent accounting for this mass of water.

### C. Phase diagrams

The miscibility of polyelectrolytes with added salts can be represented on many types of phase diagrams. The most frequent plot is salt concentration ($C_s$) versus polymer concentration ($C_p$).[7–11] We have determined these precipitation diagrams for samples *h*-NaPSS-82, *h*-NaPSS-287, *h*-NaPSS-577, and *h*-NaPSS-962 at 294 K. These diagrams are constructed by preparing a series of stock salt-containing solutions and salt-free polymer solutions, and then mixing into glass vials in a systematic fashion to furnish the library of states. The distinction of a homogeneous solution versus precipitated solutions was determined visually for a clear solution, or a white precipitate. The concentration range of these diagrams spans the dilute to semidilute and will be discussed in Sec. III A. We have probed the homogeneous phase by SANS to determine the collective and configurational properties.

The temperature dependence of polyelectrolyte phase diagrams has been explored far less.[10,26–28] Here we provide the background as to how our phase diagrams on the $T-C_p$ and $T-C_S$ coordinate planes are determined. We observed that upon heating the precipitated salty polymer solutions, they would clear leaving a clear solution. This was found to be true with exception to low polymer concentrations with high salt concentrations as the boiling point of the water preceded the clearing temperature. To provide an estimate for the phase boundaries, which would be subsequently probed by SANS, we used small-angle light scattering (SALS) and visual inspection. We observed that the SALS intensity near the phase transition became strong indicating the correlations on the order of micron length scale. To perform these experiments we used a home built SALS apparatus and hot stage.

The hot-stage used for the temperature studies accepted quartz cuvettes identical to those used for SANS. The hot-stage was made from two aluminum parts. Each part had a large volume milled such that when the two parts were fastened together, with machine screws and a paper gasket, this volume served as the reservoir for continuous flow of a recirculating fluid for the required temperature control, facilitated by drilled ports for fluid inlet and outlet. We used a PGC Scientifics heating-cooling recirculating bath with an internal fluid temperature stability of 0.1 K, using either 50:50 ethanol:water or deionized water. The sample cell was mounted into a small fitting which was accepted by the hot-stage and had a pilot hole for which a resistive thermal device (RTD) was inserted for monitoring the temperature of the sample. The stability of the sample temperature was better than 0.5 K over a 24 hour period with insulation. The hot stage had a hole drilled which allowed for the laser light to pass through the stage and thermostatically controlled quartz cuvette. The temperature of the bath was changed manually and the sample temperature recorded from the RTD controller.

The majority of the samples investigated precipitate at room temperature. The precipitation temperature upon cooling was determined by heating the sample in the hot-stage until no evidence of precipitate remained upon visual inspection and SALS. However, we observe a contribution of SALS even in the apparent high-temperature homogeneous phase, for a given $C_s$ and $C_p$. These reported precipitation temperature determined by light scattering were determined over a range of temperatures. We monitored the SALS as the temperature was lowered in decrements of 2 to 0.5 K, finer resolution in anticipation of precipitation. A minimum of 15 minutes equilibration time was used at each temperature on approach to the phase boundary. At each temperature the SALS intensity was recorded by a Princeton EG&G CCD camera in the form of the two-dimensional (2D) scattering image, or observed visually for an increase in the intensity. Either method would give an estimate for the precipitation temperature range.

One feature which we observed was that the SALS intensity would grow rapidly indicating the onset of the kinetics of precipitation. The time scales of this process often were too fast for most of the samples investigated and would be a strong function of the quench depth, polymer and salt concentrations. We restrict our interpretation of the precipitation temperature from the light scattering as an appropriate range of temperatures over which the system crossed from one in which the system in a nonprecipitated homogeneous phase to one in which the kinetics are important. Thus by the light scattering method we do not obtain the spinodal temperatures by extrapolation methods as with SANS, but by a query of whether the system is in the region of stability or evolving.

We provide an example for *h*-NaPSS-962 where the polymer concentration is 51.5 $gL^{-1}$ and salt concentration 0.19 M. In this case we were able to record a significant number of data points capturing the increase in the scattered intensity upon decrements in temperature. First with a coarse approach to determine the approximate range of temperatures and second with a longer equilibration waiting time and finer resolution. The coarse approach was equilibration at 75.4 °C for 15 minutes, followed by equilibration at 68.6 °C for equal time followed by a change to 66.0 °C. At 66 °C the scattered intensity observed visually could be seen to increase leading to precipitation. We followed this with a more elaborate approach as shown in Fig. 1. In Fig. 1(a) we dem-

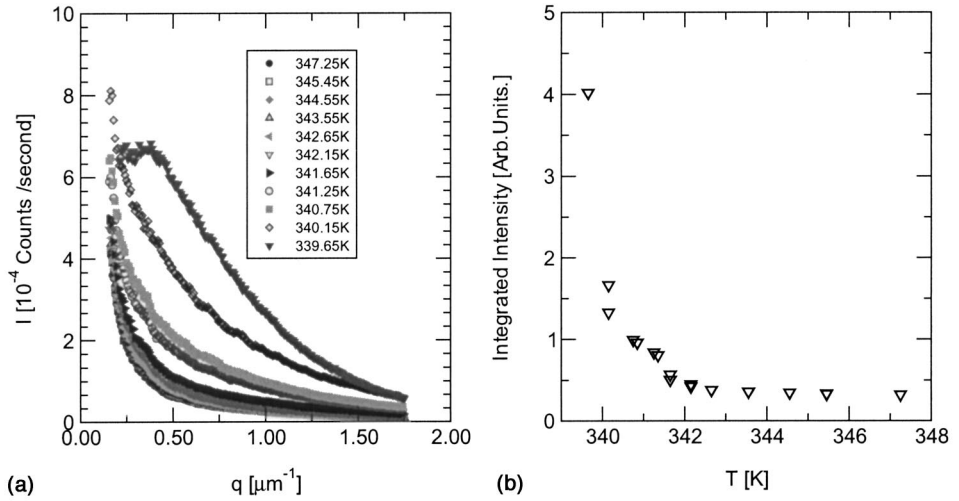


FIG. 1. (a) SALS observations for a fixed NaPSS concentration of 51.5 $gL^{-1}$, barium chloride salt concentration of 0.19 M and $N=962$. (b) Integrated scattered intensity versus temperature, same sample. The large rise in intensity at 66.5 °C is typical and indicates the phase boundary as a guide for further experiments.

onstrate on a linear plot of SALS intensity versus wave vector for several temperatures on approach to precipitation. The increase in intensity is easily observed, as well as the surprising scattering in the high temperature limit. To gain an estimate for the phase boundary we plot the integrated intensity versus temperature in Fig. 1(b) and notice the sharp increase at 339.65 K, which is marked as the phase boundary due to the onset of the kinetics. This provides empirical knowledge as to the important ranges of temperature to perform the SANS experiments. In the following figures the precipitation temperatures are extrapolated from SALS and visual inspection as the range of temperatures above the last temperature examined in which the kinetics are important. Two exceptions are the samples of polymer concentration 0.2 $gL^{-1}$ and 154.5 $gL^{-1}$ both with salt concentration 0.19 M. For the 0.2 $gL^{-1}$ sample the sample precipitation temperature could not be determined by cooling from the high temperature phase, nor with the hot stage due to the high temperatures involved. Thus, this particular sample was heated on a hot plate and visually inspected for clearing, leading to the 98.9 °C–99.8 °C result. For the sample with $C_p=154.5\ gL^{-1}$ we visually observed precipitation within the SANS spectrometer at the final observation temperature of 281.15 K.

## III. EXPERIMENTAL RESULTS

### A. Phase diagrams

The $C_s-C_p$ diagrams are shown in Fig. 2 for the system of added barium chloride ($BaCl_2$) concentration versus polyelectrolyte monomer concentration, in molar units for degree of polymerization (a) 82, (b) 287, (c) 577, and (d) 962. The filled circles represent a precipitated solution, the open circles homogeneous clear solutions. We have already shown a portion of the results for *h*-NaPSS-287 previously,[14] but here we have explored higher concentrations. Upon inspection, we find a weak $N$ dependence in these precipitation diagrams with regards to the salting-out curve. The lower molecular weight requires higher added salt to induce precipitation, a trend that is observed from $N=82$ to 962, with those limits being 0.02 M and 0.008 M, respectively.

In addition, we have explored the role of temperature on the phase behavior on several of these solutions and have discovered that the role of temperature and salt concentration are complementary. We have determined the polymer concentration dependence of the miscibility temperature, as given by the solid squares in Fig. 3, for a fixed salt concentration ($C_s=0.19$ M) and $N$ (962). The range of polymer concentration examined was 0.2 to 154 $gL^{-1}$. We did not probe the thermal dependence for lower polymer concentration due to the high temperatures involved. The solid diamonds are the spinodal temperatures determined by SANS to be discussed below.

This phase diagram is also a strong function of the salt concentration. Fixing the polymer concentration at 103 $gL^{-1}$ we examined the influence of added salt concentration on the precipitation temperatures as shown in Fig. 3(b). We observed that with increasing levels of added salt the precipitation temperature increases significantly over a small range of salt concentration, 28 K for a 0.075 M increment in salt concentration. This would suggest, in particular, for biological processes mediated by salt ions that a small change in salt concentration, or gradients, influence the thermal stability of charged macromolecules. The competing roles of ionic strength and temperature was demonstrated in a transparent manner via the Flory–Huggins treatment in our previous paper.[14]

In Figs. 3(a) and 3(b), we also present the SANS results for the phase boundary, determined by the divergence in the extrapolated scattered intensity to zero angle, $I(0)$. These data points appear within the observation range of temperatures estimated by SALS and visual inspection. The methodology for extracting the $I(0)$ is the subject of the following section, but to clarify the results for *h*-NaPSS-287 and *h*-NaPSS-577 samples, we present the SANS determined phase boundaries as well in Fig. 4. These phase diagrams are on the $T-C_s$ planes and indicate the role of increasing salt leading to an increase in the precipitation temperatures. The following results, examined by SANS total scattering, Eq. (3), probe the density–density correlations from the high

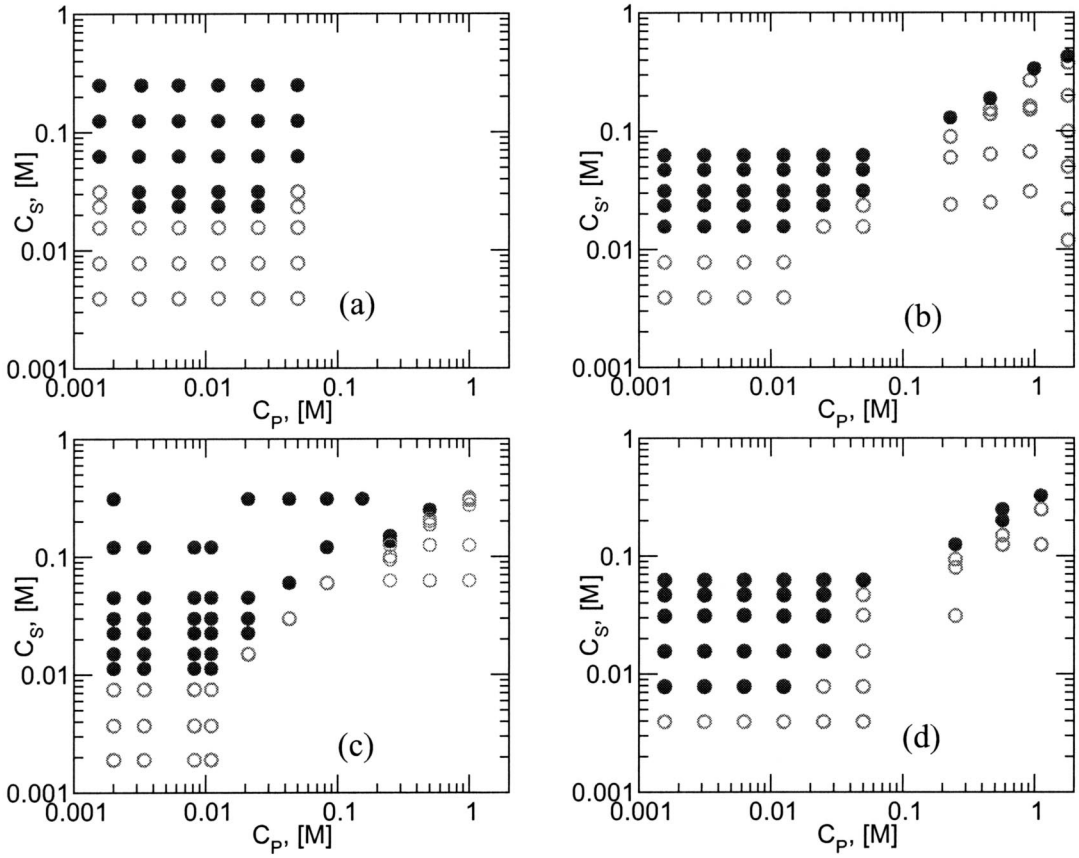


FIG. 2. Precipitation phase diagram at 294 K for several degree of polymerizations (a) 82, (b) 287, (c) 577, and (d) 962 NaPSS with added salt barium chloride.

temperature limit on approach to the relevant phase boundary by cooling.

### B. Low ionic strength: Collective properties

To build upon our previous work in which the salt-dependent phase behavior was explored we have returned to the case of low ionic strength solutions. The density–density correlations in low ionic strength polyelectrolyte solutions have long ago been measured.[29] However, this is the natural reference state before exploring the influence of added salts and temperature dependence. Thus we have explored for the case of no added salt, the density correlations as a function of degree of polymerization and polymer concentration.

Polyelectrolyte solutions at low ionic strength exhibit a peak in the total scattering structure factor at a finite wave vector $q \neq 0$. This feature is due to the presence of long-ranged electrostatic interactions and is absent in neutral homopolymer solutions which are dominated by the short-

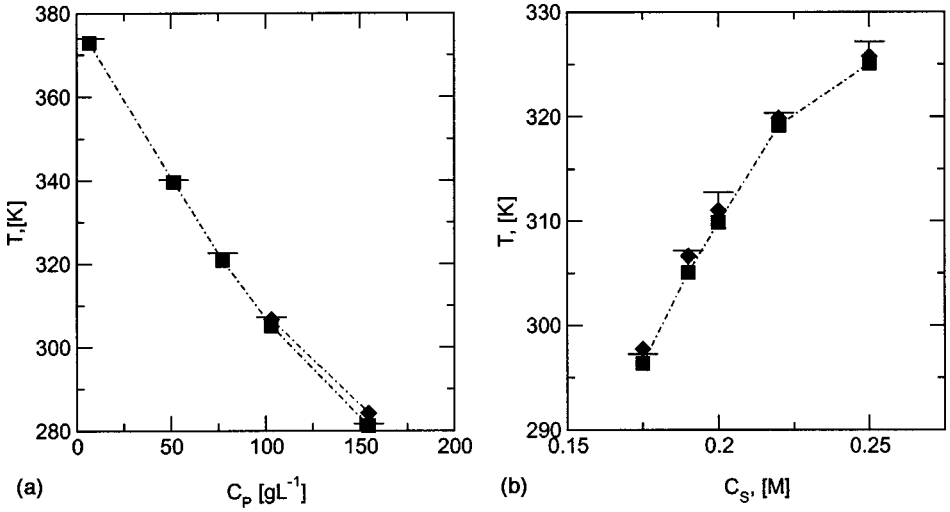


FIG. 3. (a) Influence of temperature for a fixed added salt concentration of 0.19 M, examined for $N=962$. The phase boundary by SALS (solid squares) were determined upon observation of the kinetics of the phase separation. (b) Influence of salt concentration on the precipitation temperature for a fixed polymer concentration of $C_p=103$ gL$^{-1}$ examined for $N=962$. The cloud point temperatures determined by SALS (solid squares) are systematically at lower temperatures than the SANS data (solid diamonds).

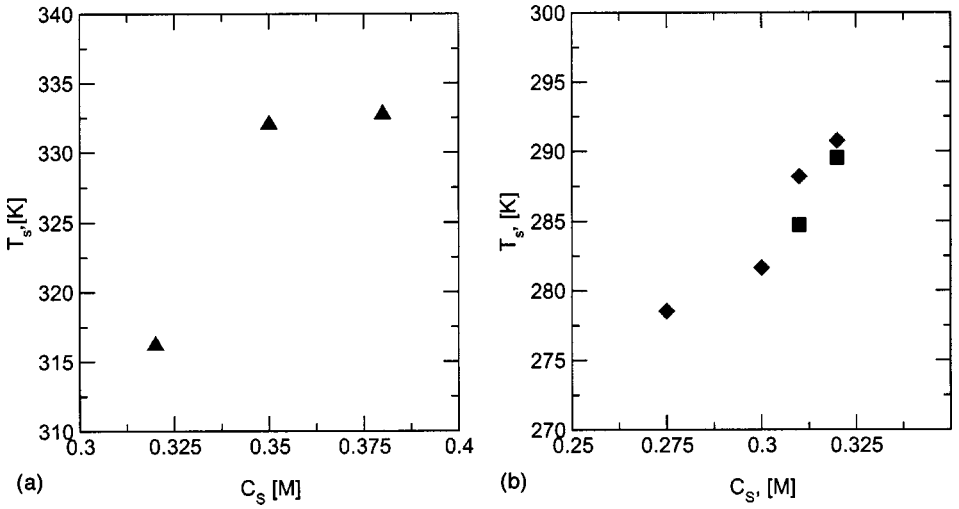


FIG. 4. Influence of extrapolated spinodal temperature for a fixed polymer concentration of 206 $gL^{-1}$, examined for $N=287$ (a) and 577 (b). The ▲ symbols are determined from the SANS experiment where the $I(0)$ are extrapolated within the Ising regime. The ■ symbols are determined by extrapolation in the Ising regime, while the ♦ is using the extrapolation in the mean field limit.

ranged interactions. Theory and simulation have predicted this polyelectrolyte peak.[30–36]

This scattering peak was investigated for flexible polyelectrolytes including poly(styrene sulfonate),[29,37,38,40] poly(*N*-methyl-2-vinyl pyridine chloride),[5] and biopolymers such as xanthan,[39] BSA,[41] and DNA.[42] The data of Kaji *et al.*[38,40] demonstrate that the inverse of the scattering wave vector ($q_{\max}^{-1}$) at the peak intensity scales with the polymer concentration as $C_p^{-1/3}$ then crosses over to $C_p^{-1/2}$, consistent with the crossovers from dilute to semidilute polyelectrolyte solutions, respectively. At even higher concentrations a narrow experimental window shows a second crossover from $C_P^{-1/2}$ to $C_p^{-1/4}$ consistent with the crossover from semidilute to concentrated regimes consistent with the double screening theory.[17] An example of the polyelectrolyte peak can be observed in the total scattering intensity at high $q$ shown in Fig. 5(a) for the no added salt case for *h*-NaPSS-577 and polymer concentration 206 $gL^{-1}$.

At the maximum intensity of the polyelectrolyte peak ($q\neq 0$) the wave vector $q_{\max}^{-1}(\equiv\xi)$ is defined and plotted versus $C_p$ in Fig. 6 for all $N$ and concentrations examined. These experimental data demonstrate the semidilute nature of the solutions, without added salts, since the correlation length appears independent of the molecular weight and varies with polymer concentration as $q_{\max}^{-1}=(73\pm 9)C_p^{-0.48\pm 0.03}$. This also suggests the proper experimental ranges in which configurational properties may be investigated in the semidilute limit. However, with the addition of salt the calculated overlap concentration ($C^\star$) would change as the chain dimensions decrease, due to screening, and possibly shift the conditions for semidilute solution to higher polymer concentrations.

Since each molecular weight has a different value for the overlap concentration, the experimental data can be reduced on a dimensionless plot of $\xi/L_C$ versus $C/C^\star$ consistent with the following scaling ansatz:

$$\xi\sim N^{\nu_{Rg}}\left(\frac{C_p}{C^\star}\right)^y, \tag{4}$$

where

$$C^\star=\frac{3M_w}{4\pi R_g^3 N_A}, \tag{5}$$

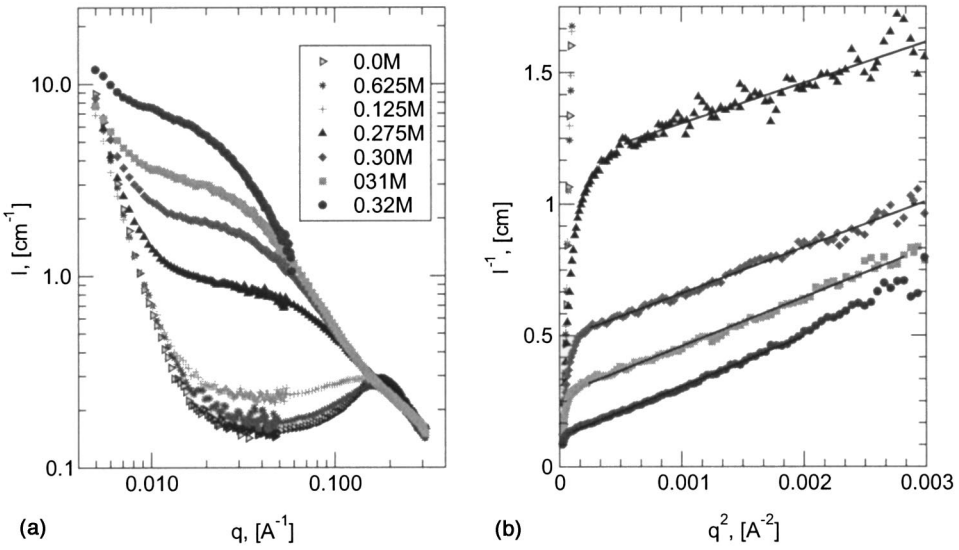


FIG. 5. (a) Typical scattered intensity versus wave vector as a function of barium chloride salt concentration for a fixed NaPSS polymer concentration of 206 $gL^{-1}$ of $N=577$ and fixed temperature of 298 K. (b) Corresponding Ornstein–Zernike plot from which $\xi$ and $I(0)$ are extracted avoiding the fit from the downturn inverse excess scattering.

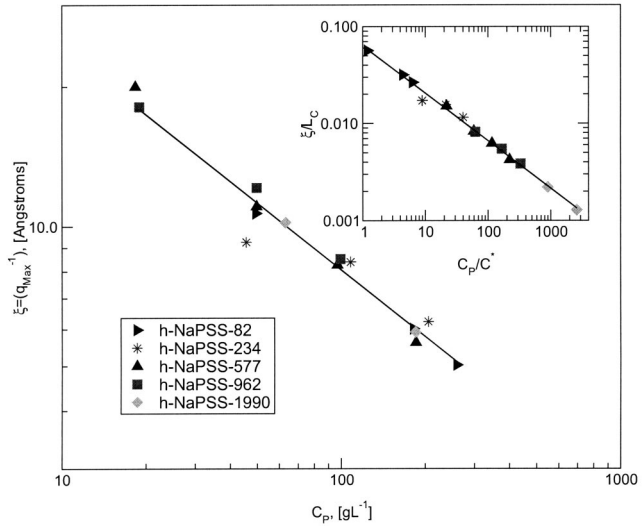


FIG. 6. Plot of inverse polyelectrolyte scattering peak ($\xi \equiv q_{\max}^{-1}$) versus polymer concentration ($C_p$), with no added salt ($T=298$ K). Regression over all raw data yields $(\xi)=(73\pm 9)\ C_p^{-0.48\pm 0.03}$. Inset, dimensionless plot of $\xi/L_C$ versus $C_p/C^\star$, using $\nu$ of 1.0 to calculate the overlap concentration ($C^\star$). Regression yields $(\xi/L_C)=(0.063\pm 0.003)(C_p/C^\star)^{-0.49\pm 0.01}$.

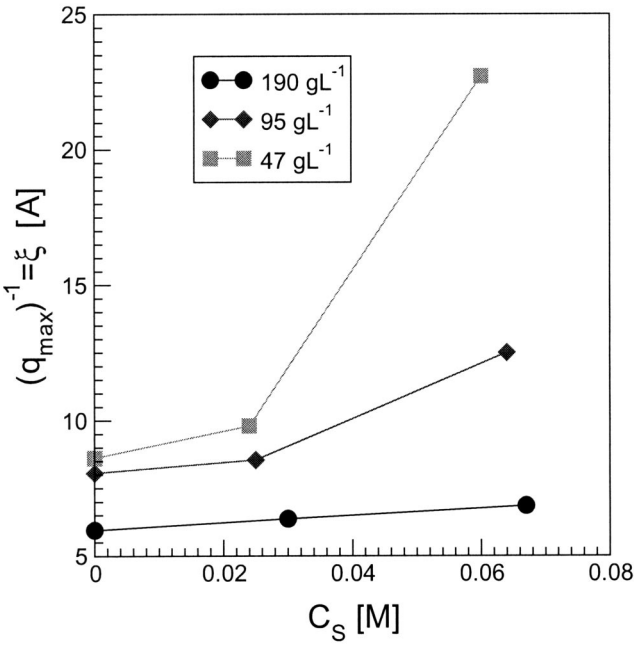


FIG. 7. Variation in inverse polyelectrolyte peak position ($q_{\max}^{-1}$) with added salt concentration for three polymer concentrations and fixed $N=234$ ($T=298$ K).

and $y$ represents the concentration scaling exponent, $N_A$ Avogadro's number, and $\nu_{Rg}$ the scaling exponent for the molecular weight dependence of the radius of gyration. Using a value for $\nu_{Rg}$ of 1.0 we estimate $C^\star$ using an extended-chain conformation (rodlike limit) for the radius of gyration and nondimensionalize the abscissa. The ordinate, hence, is dimensionless by dividing $\xi$ by the contour length ($L_C$) leading to the inset of Fig. 6. The fit over the entire range gives $(q_{\max}^{-1}/L_C)=(0.063\pm 0.003)(C_p/C^\star)^{-0.49\pm 0.01}$ over the range in degree of polymerization (82 to 1990) and concentration (18 to 300) gL$^{-1}$ consistent with the scaling ansatz and screening in semidilute polyelectrolyte solutions.

### C. High ionic strength: Collective properties

The data in Fig. 6 are results without any added salts, at a fixed temperature of 298 K and are far from precipitation phase boundaries; these solutions can be heated to near boiling and cooled to freezing without any onset of phase separation. In a previous study, Boué *et al.*[43] demonstrated that this polyelectrolyte peak had only a weak temperature dependence. This is expected since the range of correlations will increase significantly only in the proximity of a phase boundary. Hence, the correlations remain on the mesh-size length scale of semidilute solutions, familiar to that of neutral polymers,[16] but with different scaling properties. In this paper we have explored how the presence of phase boundaries leads to long-range correlations in polyelectrolyte solutions with added salt.

We have found that with the addition of salt, $\xi$ increases consistent with the results of Ise *et al.*[37] and qualitative predictions from theory.[32,33,35] The experimental data taken for degree of polymerization 234 are shown in Fig. 7, where the variation in $q_{\max}^{-1}$ with salt concentration and polymer concentration is shown. These data complement the values of the correlation length taken from the Ornstein–Zernike correlations under high salt conditions.[14] We now proceed to address the temperature dependence of the density–density correlations as the phase boundary is approached, to complement the role of added salt.

### D. Temperature dependent collective properties

Our earlier data, for varying ionic strengths at a fixed temperature, showed the divergence of $\xi$ and $I(0)$ as the precipitation phase boundary was approached.[14] This relied on fitting the data to the Ornstein–Zernike formula,

$$S_t(q)^{-1}=S_t(0)^{-1}(1+\xi^2 q^2) \tag{6}$$

for wave vectors larger than those dominated by strong excess scattering, occurring at the lowest wave vectors. The presence of this excess scattering has been verified for several molecular weights and polymer concentrations.

The new results probe the concentration fluctuations quantified by a divergence of $\xi$ and $I(0)$ with *decreasing temperature*. We examined for a fixed level of salt concentration the scattering behavior as the temperature is reduced to the point of precipitation. Similarities are observed between the temperature dependence and the salt-induced behavior. We have explored the behavior for samples *h*-NaPSS-287, *h*-NaPSS-577, and *h*-NaPSS-962. We report the main results for *h*-NaPSS-287 which directly complement our earlier results for the salt-induced precipitation.[14] The data for the remaining $N$ will follow in the discussion section.

For $N=287$, with a fixed barium chloride salt concentration of 0.38 M and fixed polymer concentration of 206 gL$^{-1}$, the scattered intensity was measured as the system was cooled from the high temperature limit to the point of macroscopic precipitation following the phase diagram presented in Fig. 4(a). The scattered intensity versus wave vector is

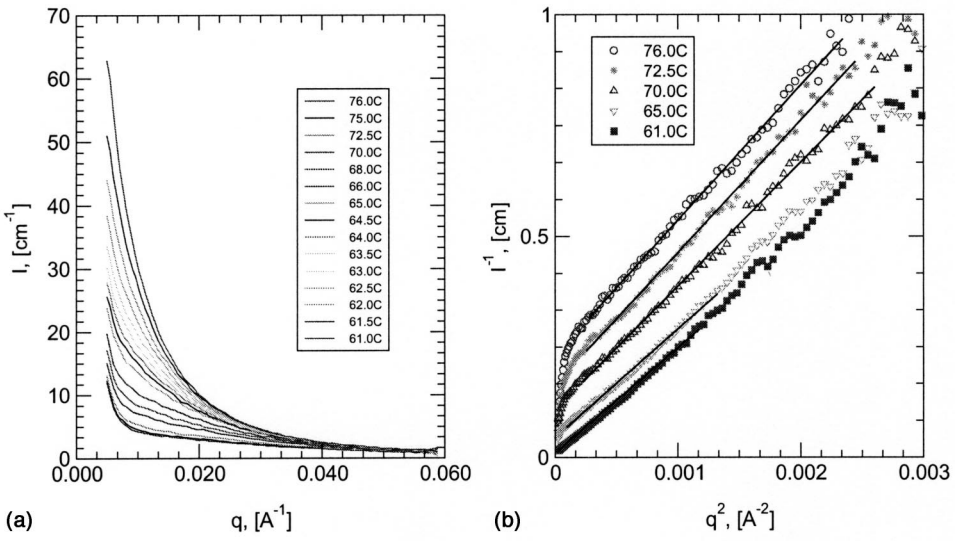


FIG. 8. (a) Typical scattered intensity versus wave vector as a function of decreasing temperature to phase boundary for a fixed NaPSS polymer concentration of 206 gL$^{-1}$ and barium chloride salt concentration 0.38 M for $N=287$. (b) Corresponding Ornstein–Zernike plot from which $\xi$ and $I(0)$ are extracted avoiding the fit to the downturn inverse excess scattering.

shown in Fig. 8(a) as well as the corresponding Ornstein–Zernike plot in Fig. 8(b). In Fig. 8(b), data for only a few temperatures are presented for clarity. Correlations of the Ornstein–Zernike type are seen by the linearity of $I(q)^{-1}$ with $q^2$ and the excess scattering deviations are observed at the low wave vectors. The systematic deviation at low $q$ becomes negligible as the temperature approaches the phase boundary. In this system, even under high salt conditions, the excess scattering remains at correspondingly high temperatures. This suggests that large scale fluctuations are present even under strong electrostatic screening. A comparison of Figs. 5 and 8 demonstrates clearly the complementary salt and temperature effects on the phase behavior of polyelectrolyte solutions.

### E. Configurational properties

We have measured the radius of gyration of labeled chains as functions of the polymer concentration and degree of polymerization, without and with added barium chloride. Examining the scattering behavior without added salt precludes the effect of the specific interactions mediated by the divalent barium ions. At the condition of the matching point, such that the coefficient $L=0$, we measured the single chain structure factor ($S_s$) from the small-angle scattering of the deuterium labeled chains. To illustrate the quality of the elimination of the total scattering, we present in Fig. 9(a) a comparison of the measured scattered intensity for the two types of experiments that measure $I_t(q)$ and $I_s(q)$ in the

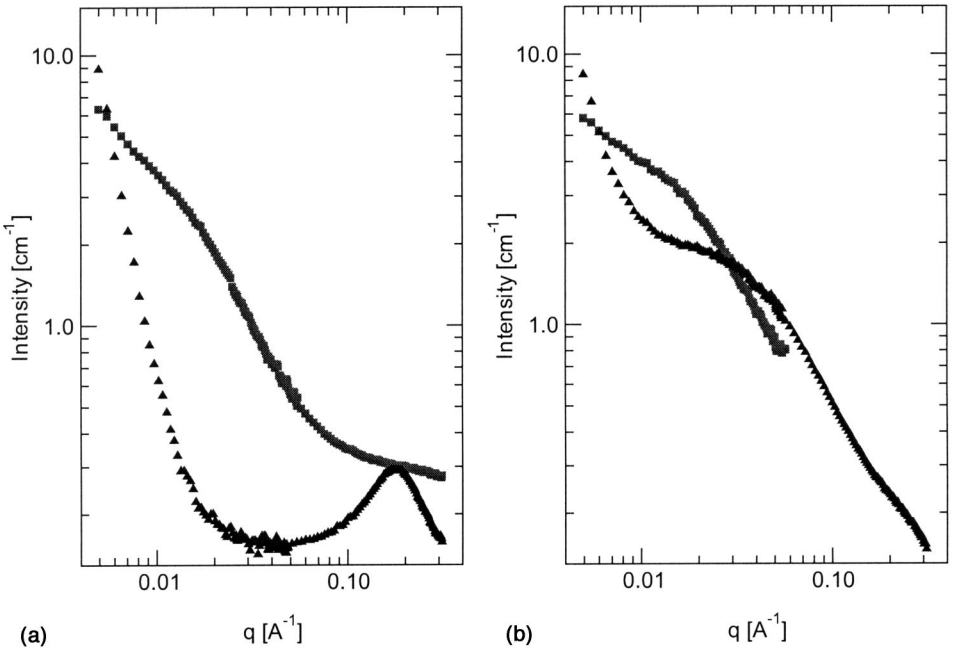


FIG. 9. Absolute intensity of total scattering (symbol ▲) and single-chain scattering (symbol ■, $N=563$, $C_P=206$ gL$^{-1}$). (a) $C_s=0.0$ M. (b) $C_s=0.30$ M. Data are not corrected for incoherent background.

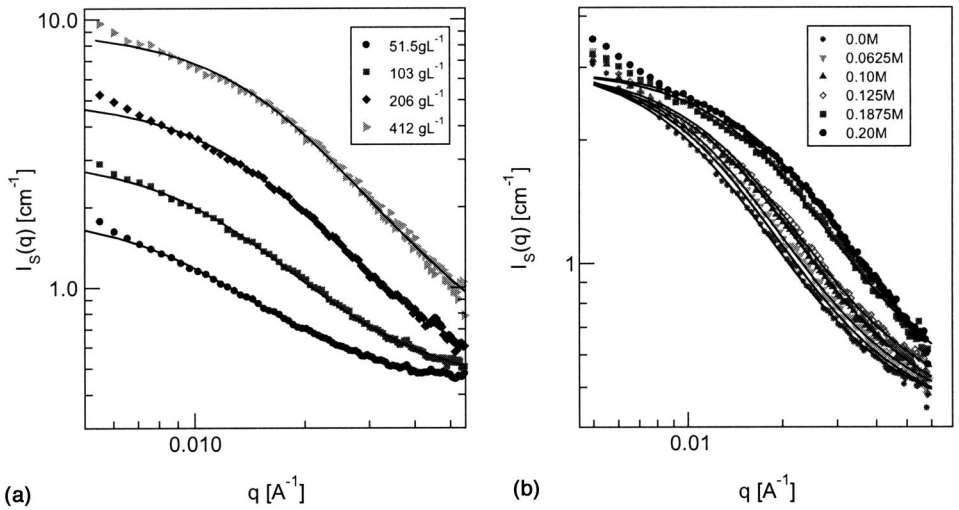


FIG. 10. (a) For a fixed $N=563$ without added salt, the measured single chain scattered intensity as a function of wave vector is shown for four different polymer concentrations. (b) Fixed polymer concentration of 103 gL$^{-1}$ and varying salt concentrations as indicated in the legend. Radius of gyration and degree of polymerization are extracted from fits to the Debye structure factor with incoherent background, shown as the dark lines.

limits of no added salt. It can be seen that contributions from the $q\neq 0$ polyelectrolyte peak are not present in the labeled chain experiment, suggesting an elimination of interchain correlations. Our data on the total scattering experiments, in the low $q$ region, show the excess scattering not predicted by current theories or simulations. For comparison we also show in Fig. 9(b) the case with high added salt of 0.30 M in which the total scattered intensity rises significantly as the high-$q$ data of $I_t$ surpasses that of $I_s$.

The results from four polymer concentrations are shown in Fig. 10(a) for *d*-NaPSS-563 on a plot of scattered intensity versus wave vector and in Fig. 10(b) the results for the same molecular weight, but at a fixed polymer concentration of 103 gL$^{-1}$ with varying levels of added salt. From these figures we extract the *Z*-averaged radius of gyration ($R_g$) by fits to the Debye structure factor, $S_D(q)$,

$$S_D(q)=\frac{2}{q^4R_g^4}(e^{-q^2R_g^2}-1+q^2R_g^2). \tag{7}$$

Clearly, the fits are excellent over most of the $q$-range studied, with exception to the lowest $q$ data. The fits from the Debye structure factor, including an incoherent background, reveal that the extrapolated scattered intensity at zero angle (and hence molecular weight) is consistent with the degree of polymerization from the GPC on the parent polystyrene as summarized in Table I. The deviation at the lowest $q$ to higher intensities is not within the experimental error of the experiment, but reflects a contribution from the total scattering. Attempts to fit the entire $q$ range including the three or four lowest data points with Eq. (7) were unsuccessful. We note that experiments performed with lower $q$ resolution would yield perfect fits to Eq. (7), but proceeding to lower $q$ may reveal deviations. The advantage with using a model form factor is that the size of the labeled chains was obtained over a wide wave vector range. Since, we did not measure the very high $q$ data, we do not extract the persistence length. Several groups[44,45] have chosen this route, but rely on a wormlike chain model to extract the persistence length, even in the semidilute condition.

## IV. DISCUSSION: TEMPERATURE DEPENDENT COLLECTIVE PROPERTIES

We now proceed with the discussion and interpretation of the SANS results. It was demonstrated earlier[14] that a mean field model for polyelectrolyte solutions leads to a modified Flory–Huggins interaction parameter such that,

$$\chi_{\text{eff}}=\chi_0-\frac{w_c}{\kappa^2}. \tag{8}$$

$\chi_0$ is the Flory–Huggins parameter for the chemical mismatch modeling the neutral hydrophobic monomer–solvent short-ranged interactions, $w_c$ represents the strength of the screened Coulombic interaction between monomers, and $\kappa^2$ is the inverse-square Debye screening length, proportional to salt concentration. $\chi_{\text{eff}}$ is the effective Flory–Huggins interaction parameter, representing the sum total chemical mismatch. Based upon this model the mean field thermodynamic behavior was predicted to have the following form for the correlation length and the extrapolated scattered intensity to zero angle:

$$\xi^{-2}\sim\left(\frac{1}{T_s}-\frac{1}{T}+\frac{w_c}{\kappa}\right)^{2\nu}$$

and (9)

$$S_t(0)^{-1}\sim\left(\frac{1}{T_s}-\frac{1}{T}+\frac{w_c}{\kappa^2}\right)^{\gamma}.$$

$T_s$ is the spinodal temperature of the corresponding neutral polymer in solution, without the influence of electrostatics and $\nu$ and $\gamma$ are the critical indices. If mean field values of $\nu$ and $\gamma$ were valid, a plot of $\xi^{-2}$ [or $S_t(0)^{-1}$] versus $1/\kappa^2$ will yield a straight line with a positive slope. Equivalently, for a fixed $1/\kappa^2$ a plot of $\xi^{-2}$ [or $S_t(0)^{-1}$] versus $1/T$ will yield a straight line with a negative slope. Deviation near the phase transition is attributed to the crossover from mean field to the Ising universality class as the role of fluctuations become important. This is the expected behavior in the limit of high salt where the electrostatic interactions become short ranged.

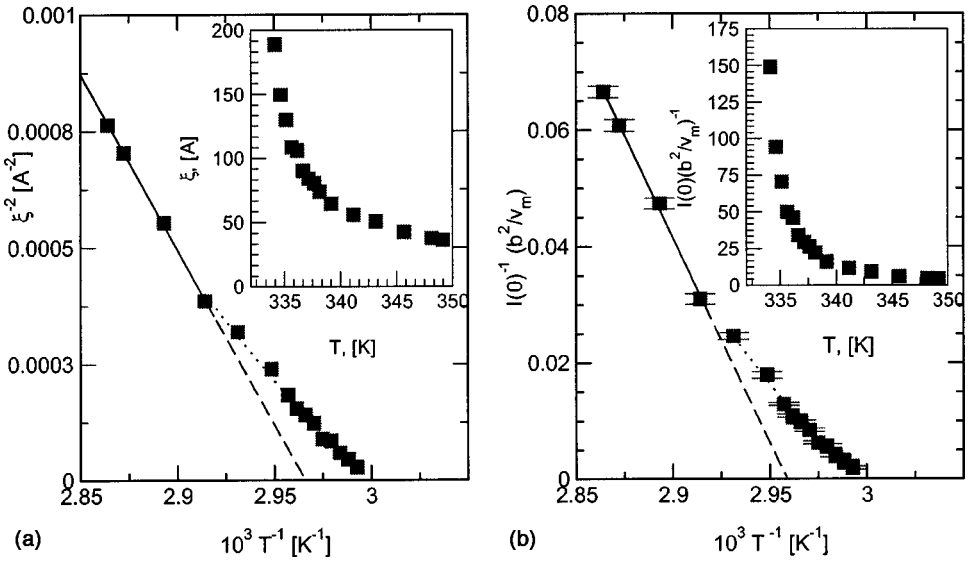


FIG. 11. Results for a fixed polymer concentration of 206 gL$^{-1}$ and salt concentration 0.38 M for $N=287$ with decreasing temperature. (a) Using a mean field plot, the solid line indicates the linear region of mean field behavior and extrapolated to the mean field spinodal temperature; and the curvature, indicated by the dotted line, shows the interpreted Ising fluctuation region; the inset shows the divergence of $\xi$ with decreasing temperature. (b) Similar mean field plot for the extrapolated-inverse scattered intensity at zero angle; the inset shows the divergence of $I(0)$. Extrapolated $T_{\mathrm{mf}}=337.94$ K and $T_{\mathrm{fluct}}=333.34$ K.

Returning to the case of *h*-NaPSS-287 we have probed the phase diagram shown in Fig. 4 that lead to the main results in Fig. 8. Now we have examined the density–density correlations quantified by the Ornstein–Zernicke formula providing the $\xi$ and $I(0)$ in the insets of Fig. 11(a) and 11(b), respectively for the fixed $C_s=0.38$ M and $C_p=206$ gL$^{-1}$. It is clearly observed that the correlation length steadily increases from 35 to near 195 Å close to the phase boundary. This significant increase was studied before in the salt-induced precipitation study. We do not have the corresponding temperature dependence of the radius of gyration data, so we can not make a comparison between $R_g$ and $\xi$. Nevertheless we note that at high temperatures the correlation length is smaller than the theta-coil and rodlike predictions, 42 Å and 200 Å, respectively.

The mean field plot provided by Eq. (9) is demonstrated in Fig. 11 in which a linear region in $1/T$ is clearly observed indicating a region of mean field applicability. This, however, is followed by the departure due to the importance of fluctuations closer to the phase transition. The fit to the mean field region is with $\nu=0.5$ and $\gamma=1.0$ and the curved line that deviates from the mean field region is fit using $\nu=0.63$ and $\gamma=1.26$, the result for the Ising universality class.[46] From Fig. 11(b), the mean field extrapolation gives the spinodal temperature of 337.94 K. By the systematic deviation from the mean field behavior the spinodal temperature is depressed to 333.34 K, a 4.6 K depression due to fluctuations.

We observed this behavior for the remaining molecular weights as well. For *h*-NaPSS-962, we examined the phase diagram displayed in Fig. 3(a) on the temperature-polymer concentration plane for $C_p=154$ gL$^{-1}$ and $C_s=0.19$ M. The Ornstein–Zernike plots display the same features as indicated for the lower molecular weight. Far from the phase transition the low-$q$ deviation is apparant, but then closer to the transition the deviation is less important as the correlation length increases. The mean field to Ising crossover in shown in Fig. 12(a) and 12(b), for $\xi$ and $I(0)$, respectively. The divergence in these quantities is given in the insets. Again, we observed the mean field region followed by systematic deviation close to the phase transition. The extrapolated mean field temperature is 289.00 K and by using the

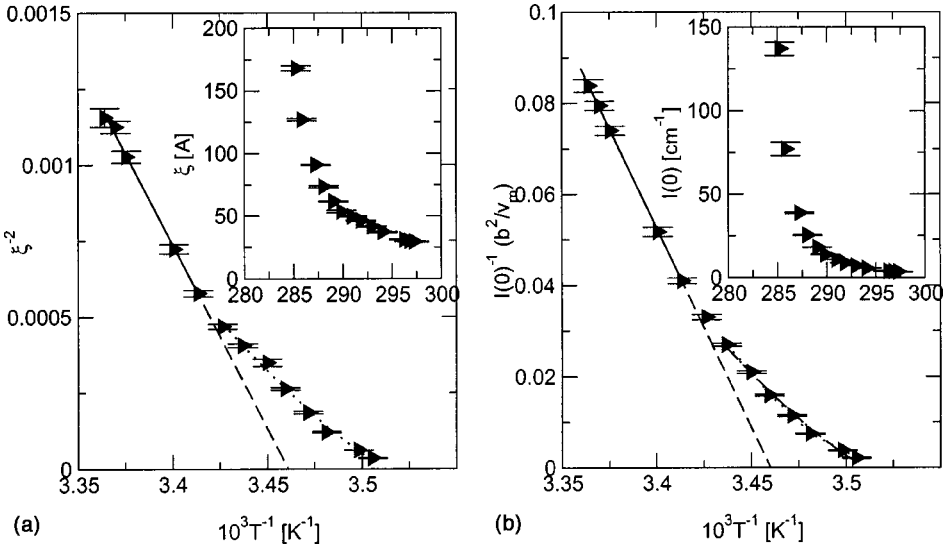


FIG. 12. Mean field fluctuation regimes, for $\xi$ (a) and $I(0)$ (b) $C_p=154$ gL$^{-1}$, $C_s=0.19$ M for $N=962$. Solid line extrapolates to $T_{\mathrm{mf}}=289.00$ K and dotted Ising fluctuation regime curve extrapolates to $T_{\mathrm{fluct}}=284.77$ K.

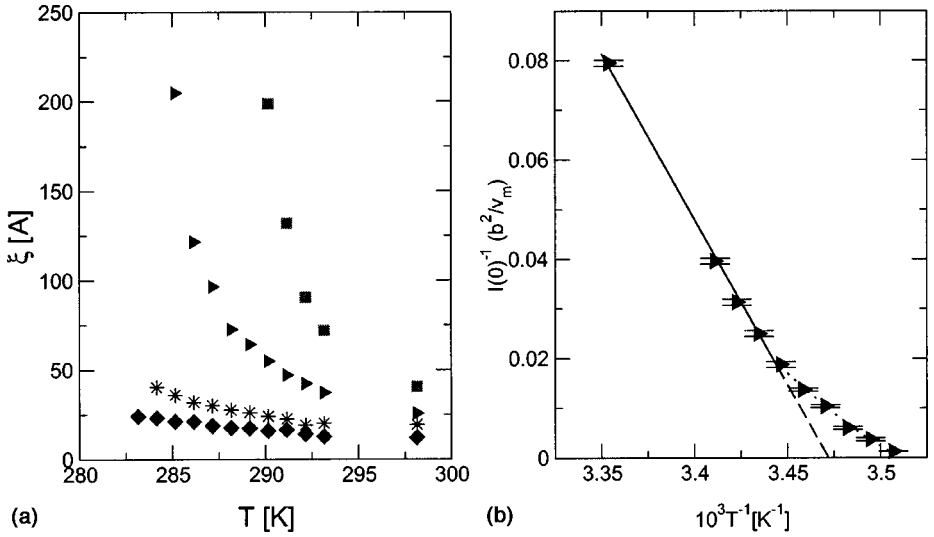


FIG. 13. (a) Divergence in the correlation length for polymer concentration 206 $gL^{-1}$ and four different added salt concentrations ■, 0.32 M; ▶, 0.31 M; *, 0.30 M; and ◆, 0.275 M. SANS experiments were performed below ambient conditions at 283 K. It was observed visually that samples with salt concentration 0.32 M and 0.31 M reached precipitation, but at the end of the experiment 0.30 M and 0.275 M were clear as reflected in the correlation lengths extracted from the resulting Ornstein–Zernike plots. (b) Mean field fluctuation crossover. $C_p = 206\ gL^{-1}$, $C_s = 0.31$ M for $N = 577$. Solid line extrapolates to $T_{mf} = 288.01$ K and dotted Ising fluctuation regime curve extrapolates to $T_{fluct} = 284.69$ K.

Ising exponent we measure the spinodal temperature to be 284.77 K, a 4.2 K depression.

We examined several solutions which were homogeneous at 294 K, but with sufficient levels of salt near the salting-out line in Fig. 2 for *h*-NaPSS-577 with polymer concentration 206 $gL^{-1}$ and varied salt concentrations 0.32, 0.31, 0.30, and 0.275 M. We show the results for the increase in the correlation length with lowering temperature to 283 K in Fig. 13(a). Two of the samples, $C_s = 0.32$ and 0.31 M, were observed to precipitate, within the allowable temperature limits, leading to diverging $I(0)$ and $\xi$. Figure 13(b) demonstrates the same analysis of Eq. (9) fitting the inverse isothermal compressibilities for the sample with salt concentration 0.31 M. The extrapolated mean field temperature is 288.01 K, while the spinodal temperature upon assuming the Ising indicies leads to 284.69 K, a 3.3 K depression.

These experimental data clearly show the crossover behavior for high salt polyelectrolyte solutions. The data support the idea that under conditions of screened electrostatics, polyelectrolyte solutions fall into the same universality class as neutral polymer solutions. The examination of critical phenomena in low ionic strength polyelectrolyte solutions is still elusive, as the appropriate experimental system has not been found. For electrolyte solutions, experimental data suggest a distinction between Coulombic criticality and solvophobic criticality.[47,48] For solvophobic criticality the system is dominated by short-range nearest neighbor interactions and displays Ising criticality very close to the critical point, as in neutral solutions. For Coulombic criticality, experimental data on different systems show either the mean field criticality[49,50] or a crossover from mean field to Ising.[48,51–53] Our results on polyelectrolyte phase behavior clearly demonstrate deviations from mean field behavior.

## V. DISCUSSION: CONFIGURATIONAL PROPERTIES

### A. Low ionic strength

The influence of added salts of type 1:1, 1:2, 1:3, etc., on the configurational properties of polyelectrolytes is complicated by specific interactions among charged species. These interactions will contribute to the phase behavior of charged macromolecules, in particular via formation of ion-pair bridging among monomers mediated by multivalent ions and condensation mechanisms. It was demonstrated that multivalent-ion-mediated interactions are necessary to observe salient features in multivalent salt-polyelectrolyte phase diagrams,[11,12,54,55] in particular the observed re-entrant or salting-in phase behavior.[7,8] However, the interpretation of these effects on the configurational properties for intrinsically flexible polyelectrolytes in nondilute solutions remains unsolved and thus the experimental data need to be demonstrated to assist in this problem.

The main results of the measured radius of gyration as a function of polymer concentration are shown in Fig. 14(a) for *d*-NaPSS-563. The four data points were fit with the regression result of $R_g = (400 \pm 28) C_p^{-0.24 \pm 0.01}$ [Å]. This result is in excellent agreement with the predictions of scaling theory and the double screening results for semidilute solutions. We also examined the influence of $N$ for a fixed polymer concentration of 206 $gL^{-1}$ as shown in Fig. 14(b). This leads to $R_g = (2.8 \pm 2.1) N^{0.6 \pm 0.1}$ [Å], where the exponent of $0.6 \pm 0.1$ is in comparison to the predicted value of 1/2. The exponent of $0.6 \pm 0.1$ suggests that the polyelectrolyte chains are quite flexible in the semidilute solution and is consistent with the single chain density–density correlation function, modeled by the Debye structure factor. However, more experiments are needed to confirm this result over a wider $N$ range. These two results combine to give the general dependence of $R_g = (9.5 \pm 9.8) C_p^{-0.24 \pm 0.01} N^{0.6 \pm 0.1}$ [Å]. We do not observe deviation from the semidilute predictions, consistent with the results from the correlation length study of Fig. 6. Further experiments are needed to examine the distinction between the semidilute and concentrated regimes. We did not analyze the structure factor in terms of a persistence length, since our data do not extend to such high $q$.

### B. High ionic strength

Consistent with our earlier investigations, we find significant coil contraction with the addition of the multivalent salt barium chloride. This coil contraction was measured for

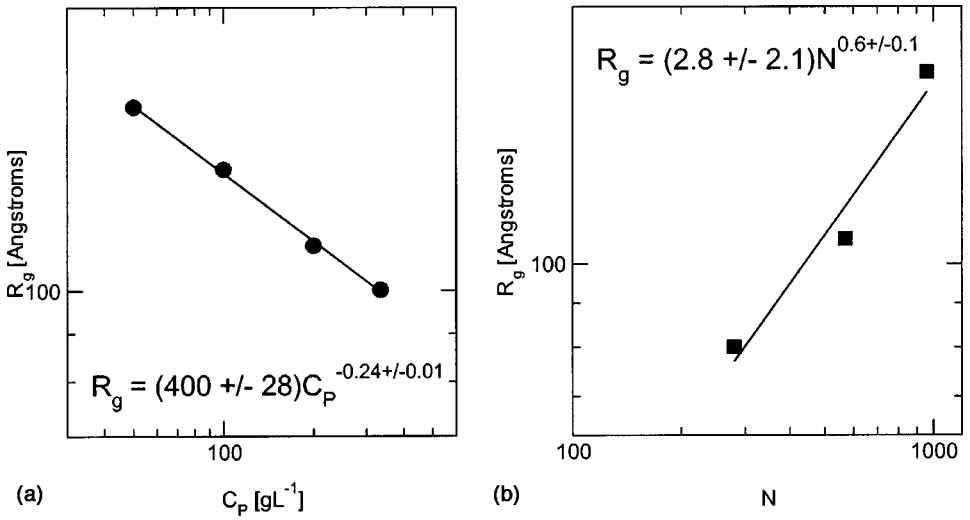


FIG. 14. Dependence of $R_g$ on polymer concentration for a fixed degree of polymerization 563 (a) and molecular weight for fixed polymer concentration of 206 $gL^{-1}$ (b).

*d*-NaPSS-274, *d*-NaPSS-563, and *d*-NaPSS-958 and polymer concentrations between 50 and 350 $gL^{-1}$, all within the semidilute regime, demonstrated earlier. Figure 15 demonstrates the main results by plotting $R_g$ and $\xi$ versus added salt concentration for $N=563$ and three polymer concentrations, 51, 103, and 206 $gL^{-1}$ as indicated in the legend. We observe a coil contraction for all concentrations and an increase in the correlation length with added salt concentration, consistent with our earlier report.[14] For the no added salt conditions the semidilute solution is observed consistent with the earlier correlation length scaling result and also by using the experimentally determined $R_g$ to calculate the overlap concentration leading to $C/C^*>1$. As the salt concentration is increased the labeled chains undergo a change by 48%, 44%, and 24% for 51, 103, and 206 $gL^{-1}$, respectively. The estimated $R_g$ values for the theta condition and extended chain conformation are 62 Å and 420 Å, respectively. In all cases the chain dimensions are well below the rodlike configurations and under high salt conditions the theta-coil dimensions are not achieved. Figure 16 shows the result for *d*-NaPSS-958. Again, the observed coil contraction is observed for polymer concentrations of 51, 103, and 206 $gL^{-1}$ as 26%, 22%, and 36.1%, respectively. The estimated $R_g$ values for the theta condition and extended chain conformation are 76 Å and 710 Å, respectively. The observed correlation lengths also increase as a function of added salt for each polymer concentration, in agreement with the earlier findings.

In the present investigation, we observe experimentally no signatures of a coil–globule transition. Precipitation precedes the expected ideal chain configuration with the increased levels of added salt which should screen the interaction. Although, this point was made earlier, we confirm this with a wider range of polymer concentration and molecular weight which concludes that even under the condition of added multivalent salt, polyelectrolytes remain swollen by excluded volume. To address these issues of excluded volume and electrostatic screening it is necessary to compare these experimental data with a theory that addresses the effect of multivalent added salt on the configuration of labeled chains in semidilute solutions. Such a theory is currently

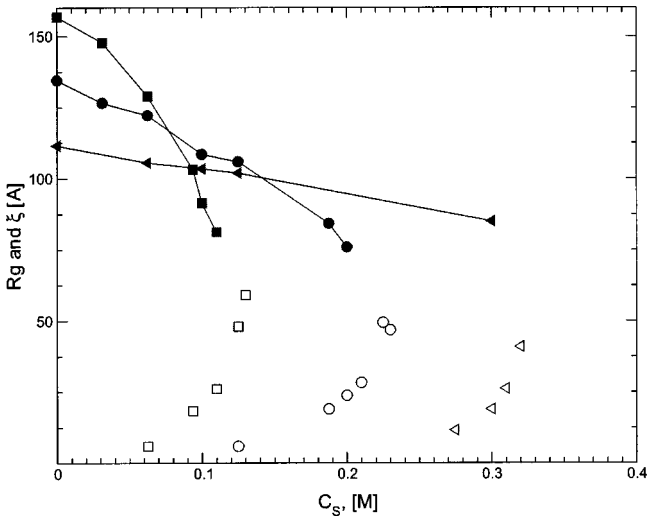


FIG. 15. Dependence of $R_g$ (filled) and $\xi$ (open) on $C_s$ for samples of matched molecular weight, *h*-NaPSS-577 and *d*-NaPSS-563. $C_p=51.5$ $gL^{-1}$ (■ and □), 103 $gL^{-1}$ (● and ○), and 206 $gL^{-1}$ (◀ and ◁).

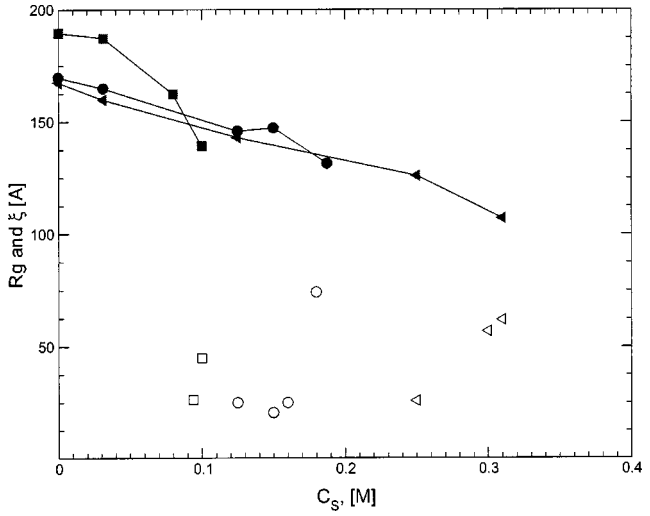


FIG. 16. Dependence of $R_g$ and $\xi$ on $C_s$ for samples *d*-NaPSS-958 and *h*-NaPSS-962. Symbols are the same as in Fig. 15.

unavailable. We hope that the present experimental results will stimulate such a theory.

## VI. CONCLUSIONS

Evidence for screening in low ionic strength polyelectrolyte solutions is found as demonstrated by the scaling of the correlation length, taken from the inverse wave vector of the $q \neq 0$ polyelectrolyte peak, with polymer concentration (in $\mathrm{gL}^{-1}$) leading to the result of $(\xi \equiv q_{\max}^{-1}) = (73 \pm 9) C_p^{-0.48 \pm 0.03}$. The exponent of 0.48 is in comparison with the scaling result of 1/2. Under the identical concentration and molecular weight ranges, the measured radius of gyration of labeled chains recovers the following results, $R_g = (400 \pm 28) C_p^{-0.24 \pm 0.01}$ and $R_g = (2.8 \pm 2.1) N^{0.6 \pm 0.1}$, using $N = 577$ and $C_p = 206\ \mathrm{gL}^{-1}$, respectively. Here, the exponents for $N$ and polymer concentration are in comparison with the theoretical values of $-1/4$ and 1/2, respectively. We have measured the crossover from the mean field to Ising criticality from the correlation length and susceptibility divergence with decreasing temperature. This crossover behavior was anticipated due to the high salt solution in which the range of the interactions is short-ranged and falls into the same universality class as neutral polymer solutions in the limit of high salt. It must be remarked that we have assumed the existence of this crossover, although we have not established the existence of a critical point in this multicomponent system. The mean field and Ising critical indices were used as an input to estimate the depression of the apparent critical temperatures due to fluctuations.

## ACKNOWLEDGMENTS

The authors are grateful to Professor D. Hoagland, G. Carri, and K. Ghosh for stimulating discussions, P. Butler for assistance with the SANS measurements at NIST and Dr. D. Schwahn for neutron beam time and hospitality in Jülich, Germany, and C. Stafford for synthesis of parent poly(styrene)s ($N = 234$, 577, and 962). V.M.P. acknowledges the financial support from a National Research Service Award T32 GM08515 from the National Institutes of Health. Acknowledgment is made to NSF Grant No. DMR 9970718 and the MRSEC at the University of Massachusetts. We acknowledge the sponsored research by the Division of Materials Science and the Laboratory Directed Research and Development Program of Oak Ridge National Laboratory, managed by UT-Battelle, LLC, for the U.S. Department of Energy under Contract No. DE-AC05-00OR22725. Experiments of Y.B.M. in Jülich were supported in part by the Alexander von Humboldt-Stiftung, Germany.

[1] K. S. Schmitz, *An Introduction to Dynamic and Static Light Scattering by Macromolecules* (Academic, New York, 1990).
[2] M. Sedlak and E. J. Amis, J. Chem. Phys. **96**, 826 (1992).
[3] M. Sedlak and E. J. Amis, J. Chem. Phys. **96**, 817 (1992).
[4] S. Förster and M. Schmidt, Adv. Polym. Sci. **120**, 51 (1995).
[5] B. D. Ermi and E. J. Amis, Macromolecules **31**, 7378 (1998).
[6] Y. Zhang, J. F. Douglas, B. D. Ermi, and E. J. Amis, J. Chem. Phys. **114**, 3299 (2001).
[7] M. Olvera de la Cruz, L. Belloni, M. Delsanti, J. P. Dalbiez, O. Spalla, and M. Drifford, J. Chem. Phys. **103**, 5781 (1995).
[8] M. Delsanti, J. P. Dalbiez, O. Spalla, L. Belloni, and M. Drifford, ACS Symp. Ser. **548**, 381 (1994).
[9] I. Michaeli, J. Polym. Sci. **48**, 291 (1960).
[10] A. Ikegami and N. Imai, J. Polym. Sci. **56**, 133 (1962).
[11] M. Axelos, M. Mestdagh, and J. Francois, Macromolecules **27**, 6594 (1994).
[12] C. Heitz and J. Francois, Polymer **40**, 3331 (1999).
[13] K. A. Narh and A. Keller, J. Polym. Sci., Part B: Polym. Phys. **31**, 231 (1993).
[14] V. M. Prabhu, M. Muthukumar, Y. B. Melnichenko, and G. D. Wignall, Polymer **42**, 8935 (2001).
[15] J. Wittmer, A. Johner, and J. F. Joanny, J. Phys. II **5**, 635 (1995).
[16] P. G. de Gennes, *Scaling Concepts in Polymer Physics* (Cornell University Press, New York, 1979).
[17] M. Muthukumar, J. Chem. Phys. **105**, 5183 (1996).
[18] C. E. Williams, M. Nierlich, J. P. Cotton *et al.*, J. Polym. Sci., Polym. Lett. Ed. **17**, 379 (1979).
[19] A. Z. Akcasu, G. C. Summerfield, S. N. Jahansan, C. C. Han, C. Y. Kim, and H. Yu, J. Polym. Sci., Polym. Phys. Ed. **18**, 863 (1980).
[20] G. D. Wignall, in *Neutron Scattering from Polymers*, edited by M. Grayson and J. Kroschwitz, Encyclopedia of Polymer Science and Engineering, 2nd ed. (Wiley, New York, 1987), Vol. 10, p. 112.
[21] W. C. Koehler, Physica (Utrecht) **137B**, 320 (1986).
[22] C. J. Glinka, J. G. Barker, B. Hammouda, S. Krueger, J. J. Moyer, and W. J. Orts, J. Appl. Crystallogr. **31**, 430 (1998).
[23] J. Schelten, in *Scattering Techniques Applied to Supramolecular and Nonequilibrium Systems*, edited by S. H. Chen, B. Chu, and R. Nossal, NATO Advanced Study Series 73 (Plenum, New York, 1981), pp. 35–48.
[24] G. D. Wignall and F. S. Bates, J. Appl. Crystallogr. **20**, 28 (1986).
[25] W. S. Dubner, J. M. Schultz, and G. D. Wignall, J. Appl. Crystallogr. **23**, 469 (1990).
[26] P. J. Flory and J. E. Osterheld, J. Phys. Chem. **58**, 653 (1954).
[27] H. Eisenberg and G. R. Mohan, J. Phys. Chem. **63**, 671 (1959).
[28] K. Nishida, M. Shibata, T. Kanaya, and K. Kaji, Polymer **42**, 1501 (2001).
[29] M. Nierlich, C. E. Williams, F. Boué *et al.*, J. Phys. (Paris) **40**, 701 (1979).
[30] P. G. de Gennes, P. Pincus, R. M. Velasco, and F. Brochard, J. Phys. (Paris) **37**, 1461 (1976).
[31] T. Odijk, Macromolecules **12**, 688 (1979).
[32] M. Grimson, M. Benmouna, and H. Benoit, J. Chem. Soc., Faraday Trans. 1 **84**, 1563 (1988).
[33] T. A. Vilgis and R. Borsali, Phys. Rev. A **43**, 6857 (1991).
[34] J.-F. Joanny and L. Leibler, J. Phys. (France) **51**, 545 (1990).
[35] J.-L. Barrat and J.-F. Joanny, Adv. Chem. Phys. **XCIV**, 1 (1996).
[36] A. Yethiraj, J. Chem. Phys. **108**, 1184 (1998).
[37] N. Ise, T. Okubo, S. Kungi, H. Matsuoka, K. Yamamoto, and Y. Ishii, J. Chem. Phys. **81**, 3294 (1984).
[38] K. Kaji, H. Urakawa, T. Kanaya, and R. Kitamaru, J. Phys. (France) **49**, 993 (1988).
[39] M. Milas, M. Rinaudo, R. Duplessix, R. Borsali, and P. Linder, Macromolecules **28**, 3119 (1995).
[40] K. Nishida, K. Kaji, and T. Kanaya, J. Chem. Phys. **114**, 8671 (2001).
[41] H. Matsuoka, N. Ise, T. Okubo, S. Kungi, H. Tomiyama, and Y. Yoshikawa, J. Chem. Phys. **83**, 378 (1985).
[42] R. Borsali, H. Nguyen, and R. Pecora, Macromolecules **31**, 1548 (1998).
[43] F. Boué, J. P. Cotton, A. Lapp, and G. Jannink, J. Chem. Phys. **101**, 2562 (1994).
[44] M. N. Spiteri, F. Boué, A. Lapp, and J. P. Cotton, Phys. Rev. Lett. **77**, 5218 (1996).
[45] E. Dubois and F. Boué, Macromolecules **34**, 3684 (2001).
[46] P. M. Chaikin and T. C. Lubensky, *Principles of Condensed Matter Physics* (Cambridge University Press, Cambridge, 1995).
[47] M. E. Fisher, J. Stat. Phys. **75**, 1 (1994), and references therein.
[48] T. Narayanan and K. S. Pitzer, J. Chem. Phys. **102**, 8118 (1995).
[49] R. R. Singh and K. S. Pitzer, J. Chem. Phys. **92**, 6775 (1990).
[50] K. C. Zhang, M. E. Briggs, R. W. Gammon, and J. M. H. Levelt Sengers, J. Chem. Phys. **97**, 8692 (1992).
[51] P. Chieux and M. J. Sienko, J. Chem. Phys. **53**, 566 (1970).
[52] S. Wiegand, M. E. Briggs, J. M. H. Levelt Sengers, M. Kleemeier, and W. Schröer, J. Chem. Phys. **109**, 9038 (1998).
[53] H. Weingärtner, S. Wiegand, and W. Schröer, J. Chem. Phys. **96**, 848 (1992).
[54] J. Francois, C. Heitz, and M. Mestdagh, Polymer **38**, 5321 (1997).
[55] I. Sabbagh and M. Delsanti, Eur. Phys. J. E **1**, 75 (2000).